Stabilizing Angle Rigid Formations With Prescribed Orientation and Scale

Liangming Chen, *Member, IEEE*, Qingkai Yang, *Member, IEEE*, Mingming Shi, Yanan Li, and Mir Feroskhan

***Abstract*—Angle rigid formations have the advantage of requiring only local bearing/direction measurements in their implementation. However, the capability of controlling the orientation and scale of these formations has not been explored. This undetermined orientation and scale can degrade the robustness of the formation against measurement noise. To maintain both advantages of requiring less sensor measurements and sustaining robustness against measurement noise, this article aims to achieve a desired angle rigid formation while simultaneously controlling its orientation and scale. In this article, we first design a formation algorithm for the first three agents to achieve a desired triangular formation with prescribed orientation and scale. Using the control gain design technique, we then design formation control algorithms for the remaining agents such that the overall desired formation can be achieved under a vertex addition operation. We present the role of *generic* property from angle rigidity for the formation's stability analysis. We also highlight that with one additional relative position measurement or two additional communication channels, the local convergence to the corresponding desired formation can be improved to a global convergence. Experiments are conducted to validate the theoretical results and the advantages are highlighted in comparison with other two formation control laws.**

***Index Terms*—Bearing/direction measurement, formation control, multiagent systems, prescribed orientation and scale, angle rigidity.**

I. Introduction

MULTIAGENT formation control has been extensively studied recently due to its broad applications in robotic transportation in smart factories [1], drone light shows [2], and satellite formation flying for Earth observation [3], to name a few. The aim of multiagent formations is to control a group of agents to form a desired geometric shape, which can be described by absolute positions, relative positions, distances, bearings, or angles [4]. When the absolute position can be measured via a global positioning system (GPS), the position-based control algorithm can globally stabilize the formation. Since precise global positioning is expensive and unavailable in a GPS-denied environment, the local sensing-based formation approaches are more favored [4]–[9], which mainly include relative position-based approach, distance-based approach, bearing-based approach, and angle-based approach.

When the orientations of all the agents' coordinate frames are the same, the relative position-based formation control algorithms can also globally stabilize a formation. However, it is relatively difficult to precisely align all agents' coordinate frames due to the existence of sensing noise and disturbances. When a small misalignment on agents' coordinate frames exists, the formation will be distorted and an additional translational motion will emerge [10], which is undesirable in engineering practices [8]. To increase the robustness against the misalignment of agents' coordinate frames, a distance-based formation approach [11]–[13] can be employed using the theoretical tool of distance rigidity [12], [14], which allows each agent to have its own local coordinate frame to measure relative positions. Although the sensors for the alignment of agents' coordinate frames, such as compasses, are not required in the distance-based formation approach, most of the distance-based formation control algorithms can only stabilize the formation locally.

To further reduce the sensor equipment, the bearing formation approach has been studied based on the bearing rigidity theory [6]. Instead of using relative position measurements, the developed formation algorithms in [6] and [15] only require bearing measurements, which can be acquired from cameras, sonars, and sensors array [16]. Since bearing is a vector whose description relies on a coordinate frame, the bearing formation algorithms also require the alignment of all agents' coordinate frames. Unlike the bearing formation approach, angle formation approach that is based on angle rigidity requires only bearing measurements but allows all agents to have their own coordinate frames to measure their respective bearings independently. This is because the spanned angles among agents are invariant to the orientations of the agents' coordinate frames. However, the orientation and scale of the angle rigid formations are

Manuscript received June 6, 2021; revised September 6, 2021; accepted September 28, 2021. Date of publication October 21, 2021; date of current version June 6, 2022. The work of Q. Yang was supported by the National Natural Science Foundation of China under Grant 61903035, and the work of M. Shi was supported by the "RevealFlight" Concerted Research Action (ARC) of the Federation Wallonie-Bruxelles. *(Corresponding author: Mir Feroskhan.)*

Liangming Chen and Mir Feroskhan are with the School of Mechanical and Aerospace Engineering, Nanyang Technological University, Singapore 639798 (e-mail: liangming.chen@ntu.edu.sg; mir.feroskhan@ntu.edu.sg).

Qingkai Yang is with the School of Automation, Beijing Institute of Technology, Beijing 100081, China (e-mail: qingkai.yang@bit.edu.cn).

Mingming Shi is with the ICTEAM Institute, UC Louvain, 1348 Louvain-la-Neuve, Belgium (e-mail: m.shi@uclouvain.be).

Yanan Li is with the School of Astronautics, Harbin Institute of Technology, Harbin 150001, China (e-mail: liyanan@hit.edu.cn).

Color versions of one or more figures in this article are available at https://doi.org/10.1109/TIE.2021.3120476.

Digital Object Identifier 10.1109/TIE.2021.3120476

undetermined [7], [17], which degrades the formation's robustness against noise and hampers the execution of some practical tasks, such as obstacle avoidance during multirobot search and rescue. To acquire both advantages of angle rigid formations and robustness against noise, one can enforce constraints on orientation and scale into the angle rigid formations.

Motivated by the aforementioned works, we aim to achieve a desired angle rigid formation with prescribed orientation and scale and simultaneously minimize the sensor measurements to reduce the system cost. First, to reduce the requirement on sensor equipment, we describe the desired formation by using interior angles, which allow agents to have their own local coordinate frames. To guarantee that the achieved formation is unique, the angle-described formation is required to be *angle rigid*, which can be constructed by first determining a triangular formation for the first three agents. Subsequently, the remaining agents are sequentially added into the desired formation using a vertex addition operation, in which two new angle constraints associated with the added agent will be specified. Therefore, the orientation and scale of the whole formation can be controlled by the first three agents' triangular formation. Compared to the previous results, the key contributions of this work lie in three aspects.

1) By imposing relative position constraints to the first triangular formation, the angle rigid formation is stabilized with prescribed orientation and scale, which provides the formation with more robustness against noise than the angle rigid formations in [7] and [17].
2) By using a control gain design technique, a more general angle formation algorithm is designed. We show that the *generic* property of the agents' desired formation configuration plays an important role in the control gain selection of the formation law. As compared to the earlier work [17], the designed control law can stabilize all the generic formations.
3) As compared to [7], [15], and [17], we also show that with one additional relative position measurement on the first three agents or two additional communication channels on each of the other agents, the local convergence to their corresponding desired formation can be improved to a global convergence. Moreover, most of the agents can implement their control laws in their own local coordinate frames.

The rest of this article is organized as follows. Section II presents the preliminaries and problem formulation. Section III introduces the control of the first three agents. In Section IV, the extension to the remaining agents is investigated.

II. Preliminaries and Problem Formulation

A. Agents' Dynamics

Consider a group of $N (N \geq 4)$ agents in the plane labeled from 1 to N. Each agent i is governed by the single-integrator dynamics

$$\dot{p}_i = u_i, i = 1, \dots, N \tag{1}$$

where $p_i \in \mathbb{R}^2$ denotes agent i's position described in a fixed global coordinate frame $\sum_g$ and $u_i \in \mathbb{R}^2$ is the control input.

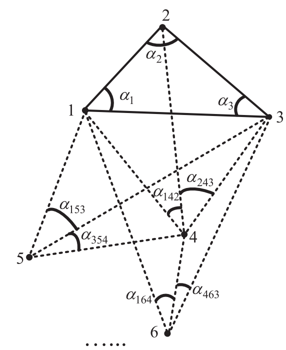

Fig. 1. Formation construction starting from a triangular shape.

B. Construction of the Desired Angle Rigid Formations

Define bearing $b_{ij} := \frac{p_j - p_i}{\|p_j - p_i\|}$ as the unit vector starting from p_i and pointing toward p_j, $p_i \neq p_j$. The interior angle α_{kij} can be computed as $\alpha_{kij} := \measuredangle kij = \arccos(b_{ij}^{\mathrm{T}} b_{ik}) \in [0, \pi]$ which is independent of the orientation of the agent i's coordinate frame. We describe the desired formation by a set of interior angles. To guarantee the achieved formation unique, we aim to control those multiagent formations that are angle rigid. A planar formation that consists of a set of agents and angle constraints among them is said to be *angle rigid* if under appropriately chosen angle constraints, the formation can only translate, rotate, or scale as a whole when one or more of their positions are perturbed locally. An angle rigid formation with the configuration $p = [p_1^{\mathrm{T}}, \dots, p_N^{\mathrm{T}}]^{\mathrm{T}} \in \mathbb{R}^{2N}$ being generic, that is, no three agents are collinear and no four agents are on a circle, is said to be *generically angle rigid*. For more details about angle rigidity, readers can refer to [17].

To construct a generically angle rigid N-agent formation as shown in Fig. 1, according to the Type-I vertex addition operation in [17], one can grow the formation by the following $N-2$ steps.

Step 1: One constructs the first triangular formation $\triangle 123$ using three angle constraints: $\measuredangle 123, \measuredangle 231$, and $\measuredangle 312$.

Step 2: One adds agent 4 under the two angle constraints: $\measuredangle 214$ and $\measuredangle 124$ (in this case 1, agent 4 has two neighbors 1, 2), or $\measuredangle 142$ and $\measuredangle 243$ (in this case 2, agent 4 has three neighbors 1, 2, 3).

...

Step k-2: One adds agent k under the two angle constraints: $\measuredangle j_1 k j_2$ and $\measuredangle j_2 k j_3$, $j_1, j_2, j_3 \in \{1, \dots, k-1\}$, or $\measuredangle j_1 j_2 k$ and $\measuredangle j_2 j_1 k$.

...

Step N-2: One adds agent N under the two angle constraints: $\measuredangle i_1 N i_2$ and $\measuredangle i_2 N i_3$, or $\measuredangle i_1 i_2 N$ and $\measuredangle i_2 i_1 N$.

To guarantee the uniqueness of each agent's position in step 2 to step $N-2$ under the given two angle constraints, the following assumption is needed.

Assumption 1: In the aforementioned step $k, k = 2, \dots, N-2$ with the corresponding newly added agent i and its angle constraints $\measuredangle j_1 i j_2$ and $\measuredangle j_2 i j_3$, we assume that the positions of $\{i, j_1, j_2, j_3\}$ are generic.

Remark 1: In Assumption 1, if $\{i, j_1, j_2, j_3\}$ are not generic, agent i cannot be uniquely added because, for example, when $p_i, p_{j_1}, p_{j_2}, p_{j_3}$ are cocircle, p_i and $\measuredangle ij_1j_2$ are not unique under the given two angle constraints. The formation's orientation and scale are important in many missions, such as multiagent search and rescue. However, the agents are also required to equip other payloads to achieve the corresponding tasks and, thus, have limited space for equipping bulky sensors to achieve the desired formation. Therefore, we will only apply further constraints to the first triangle such that the prescribed orientation and scale of the whole formation can be achieved by the first three agents, and the remaining agents only need to equip light bearing sensors to achieve their desired formation.

C. Control Objective

Based on the construction steps given in Section II-B, we first aim at achieving the desired triangular shape and then adding the remaining agents one at a time to the existing formation. Specifically, for agents 1–3, the aim is to achieve

$$\lim_{t\to\infty} e_1(t) = \lim_{t\to\infty}(p_1(t) - p_2(t) - \delta_{21}) = 0, \quad (2)$$

$$\lim_{t\to\infty} e_2(t) = \lim_{t\to\infty}(p_2(t) - p_3(t) - \delta_{32}) = 0, \quad (3)$$

$$\lim_{t\to\infty} e_3(t) = \lim_{t\to\infty}(p_3(t) - p_1(t) - \delta_{13}) = 0 \quad (4)$$

where $\delta_{ij} \in \mathbb{R}^2$ is the desired relative position of agent j with respect to agent i, which determines not only the orientation and scale of the triangle but also the interior angles since $\alpha^*_{jik} = \arccos\left(\frac{\delta_{ij}^\top}{\|\delta_{ij}\|}\frac{\delta_{ik}}{\|\delta_{ik}\|}\right), i, j, k \in \{1, 2, 3\}$. Note that δ_{21}, δ_{32}, and δ_{13} are redundant to describe a triangle with prescribed orientation and scale since $\delta_{21} = -\delta_{32} - \delta_{13}$ and $\alpha^*_{312} + \alpha^*_{123} + \alpha^*_{231} = \pi$. Therefore, it is unnecessary for agents 1–3 to have relative position measurements at the same time to achieve (2)–(4). For agents 4–N, if each of them has three neighbors (case 2), the aim is to achieve

$$\lim_{t\to\infty} e_{i1}(t) = \lim_{t\to\infty}(\alpha_{j_1ij_2}(t) - \alpha^*_{j_1ij_2}) = 0, \quad (5)$$

$$\lim_{t\to\infty} e_{i2}(t) = \lim_{t\to\infty}(\alpha_{j_2ij_3}(t) - \alpha^*_{j_2ij_3}) = 0 \quad (6)$$

where $i = 4, \ldots, N$, $j_1 < i, j_2 < i, j_3 < i$, and $\alpha^*_{j_1ij_2} \in (0, \pi), \alpha^*_{j_2ij_3} \in (0, \pi)$ denote agent i's two desired angles formed with three neighboring agents $j_1, j_2, j_3 \in \{1, 2, \ldots, i-1\}, j_1 \neq j_2 \neq j_3$. If each of the agents 4–N has two neighbors (case 1), the aim is to achieve

$$\lim_{t\to\infty} \bar{e}_{i1}(t) = \lim_{t\to\infty}(\alpha_{j_1j_2i}(t) - \alpha^*_{j_1j_2i}) = 0, \quad (7)$$

$$\lim_{t\to\infty} \bar{e}_{i2}(t) = \lim_{t\to\infty}(\alpha_{j_2j_1i}(t) - \alpha^*_{j_2j_1i}) = 0 \quad (8)$$

where $\alpha^*_{j_1j_2i} \in (0, \pi), \alpha^*_{j_2j_1i} \in (0, \pi)$.

To show the control objectives we will achieve in the follow-up sections, we summarize them as the flow graph in Fig. 2.

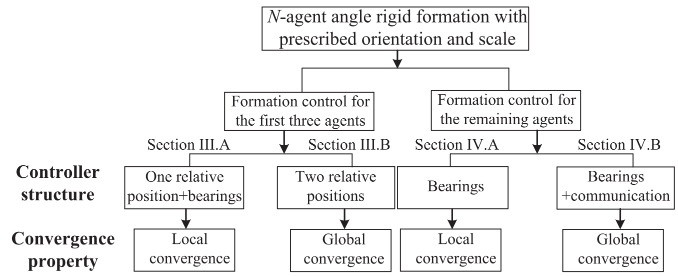

Fig. 2. Overall structure of the follow-up sections and their relationship.

III. Formation Control for the First Three Agents

To achieve (2)–(4), we first design a locally stable formation law using the minimum number of relative position measurement. To improve the convergence capability to the desired formation, we then design a globally stable formation law, in which one more relative position measurement is needed.

A. Local Stabilization Using One Relative Position Measurement

Different from the proposed algorithm in [17] where the orientation and scale of the triangular formation is undetermined, we now aim at achieving the triangular formation with prescribed orientation and scale using one relative position measurement for agent 1 and bearing measurements for agents 2 and 3. We design the control laws for agents 1–3 as

$$u_1 = -k_1(p_1 - p_2 - \delta_{21}) = -k_1e_1, \quad (9)$$

$$u_2 = -k_2(\alpha_2 - \alpha_2^*)b_{21} = -k_2\bar{e}_2b_{21}, \quad (10)$$

$$u_3 = -k_3(\alpha_3 - \alpha_3^*)b_{32} = -k_3\bar{e}_3b_{32} \quad (11)$$

where $k_i, i \in \{1, 2, 3\}$ are positive scalars, $\bar{e}_j = \alpha_j - \alpha_j^*, j = 2, 3$, and α_i represents $\alpha_{[i-1]i[i+1]}, [4] = 1, [0] = 3, [i] = i, i = 1, 2, 3$ for conciseness. The control laws (9)–(11) represent that agent 1 will maintain the desired relative position δ_{21} with respect to agent 2, and agents 2 and 3 will maintain the desired angles α_2^* and α_3^*, respectively. Correspondingly, agent 1 will measure relative position $p_1 - p_2$ using, e.g., radar, and agents 2 and 3 measure bearings using, e.g., camera. Note that the orientation of the triangular formation is determined by $\delta_{21}/\|\delta_{21}\|$ and the scale is determined by $\|\delta_{21}\|$.

Theorem 1: For a three-agent formation (1) governed by (9)–(11), if the initial errors $\|p_i(0) - p_j(0) - \delta_{ji}\|, i, j = 1, 2, 3$ are small, the formation objective (2)–(4) can be achieved and the formation errors $e_i(t)$ asymptotically converge to zero.

Proof: To obtain the convergence of e_i, we first need to derive their dynamics. First, one has

$$\dot{e}_1 = \dot{p}_1 - \dot{p}_2 = -k_1e_1 + k_2\bar{e}_2b_{21}. \quad (12)$$

To derive the dynamics of $\dot{e}_2$, we consider two different ways to describe its time-derivative

$$\frac{\mathrm{d}\cos\alpha_{ijk}}{\mathrm{d}t} = (-\sin\alpha_{ijk})\dot{\alpha}_{ijk} = \dot{b}_{ji}^{\mathrm{T}}b_{jk} + b_{ji}^{\mathrm{T}}\dot{b}_{jk}$$
$$= \left[\frac{P_{b_{ji}}}{l_{ji}}(\dot{p}_i - \dot{p}_j)\right]^{\mathrm{T}} b_{jk} + b_{ji}^{\mathrm{T}}\frac{P_{b_{jk}}}{l_{jk}}(\dot{p}_k - \dot{p}_j) \quad (13)$$

where $l_{jk} = \|p_j - p_k\|$, $P_{b_{ji}} = I_2 - b_{ji}b_{ji}^{\mathrm{T}}$. It follows that

$$\dot{\alpha}_{ijk} = -\left[\frac{P_{b_{ji}}}{l_{ji}\sin\alpha_{ijk}}(\dot{p}_i - \dot{p}_j)\right]^{\mathrm{T}} b_{jk} - b_{ji}^{\mathrm{T}}\frac{P_{b_{jk}}}{l_{jk}\sin\alpha_{ijk}}(\dot{p}_k - \dot{p}_j). \tag{14}$$

For the cases of $ijk = 123$ and $ijk = 231$, substituting (9)–(11) into (14) yields

$$\begin{aligned}\dot{\bar{e}}_2 &= -\left[\frac{P_{b_{23}}}{l_{23}\sin\alpha_2}(\dot{p}_3 - \dot{p}_2)\right]^{\mathrm{T}} b_{21} - b_{23}^{\mathrm{T}}\frac{P_{b_{21}}}{l_{21}\sin\alpha_2}(\dot{p}_1 - \dot{p}_2)\\ &= k_1\frac{b_{23}^{\top}P_{b_{21}}}{l_{21}\sin\alpha_2}e_1 - k_2\frac{\sin\alpha_2}{l_{23}}\bar{e}_2 \end{aligned}\tag{15}$$

$$\begin{aligned}\dot{\bar{e}}_3 &= -\left[\frac{P_{b_{32}}}{l_{32}\sin\alpha_3}(\dot{p}_2 - \dot{p}_3)\right]^{\mathrm{T}} b_{31} - b_{32}^{\mathrm{T}}\frac{P_{b_{31}}}{l_{31}\sin\alpha_3}(\dot{p}_1 - \dot{p}_3)\\ &= -k_3\frac{\sin\alpha_3}{l_{31}}\bar{e}_3 + k_1\frac{b_{32}^{\top}P_{b_{31}}}{l_{31}\sin\alpha_3}e_1 + k_2\frac{\sin\alpha_2}{l_{32}}\bar{e}_2. \end{aligned}\tag{16}$$

Letting $e_f = [e_1^{\top}, \bar{e}_2, \bar{e}_3]^{\top}$ and then summarizing (12)–(16), one has the overall dynamics

$$\dot{e}_f = \begin{bmatrix} -k_1 I_2 & k_2 b_{21} & 0 \\ k_1 g_{321} & -k_2 f_{23} & 0 \\ k_1 g_{231} & k_2 f_{23} & -k_3 f_{31}\end{bmatrix}\begin{bmatrix} e_1 \\ \bar{e}_2 \\ \bar{e}_3\end{bmatrix} = A_1(e_f)e_f \tag{17}$$

where $g_{ijk} = \frac{b_{ji}^{\top}P_{b_{jk}}}{l_{jk}\sin\alpha_j} \in \mathbb{R}^{1\times 2}$, $f_{ij} = \frac{\sin\alpha_i}{l_{ij}} \in \mathbb{R}$, $A_1(e_f) \in \mathbb{R}^{4\times 4}$. Note that the dynamics (17) is highly nonlinear due to the state-dependent matrix $A_1(e_f)$. Thus, the global stability analysis of (17) is quite challenging. Now, we conduct the local stability analysis for dynamics (17) using the linearization technique. Around the desired equilibrium $\{e_1 = 0, \bar{e}_2 = 0, \bar{e}_3 = 0\}$, we check the Jacobian of (17). Taking e_1 as an example, one has

$$\begin{aligned}\dot{e}_1 &= \left(\frac{\partial(-k_1e_1 + k_2\bar{e}_2b_{21})}{\partial e_1}|_{e_f=0}\right)e_1 + \left(\frac{\partial(-k_1e_1 + k_2\bar{e}_2b_{21})}{\partial\bar{e}_2}|_{e_f=0}\right)\bar{e}_2\\ &= \left(\left(-k_1I_2 + k_2\bar{e}_2\frac{\partial b_{21}}{\partial e_1}\right)|_{e_f=0}\right)e_1 + \left(k_2b_{21}|_{e_f=0}\right)\bar{e}_2.\end{aligned}\tag{18}$$

Now we calculate $\frac{\partial b_{21}}{\partial e_1}$ in (18). Note that

$$\frac{\partial b_{21}}{\partial e_1} = \frac{\partial\frac{e_1+\delta_{21}}{\|e_1+\delta_{21}\|}}{\partial e_1} = \frac{I_2\|e_1+\delta_{21}\| - (e_1+\delta_{21})\frac{(e_1+\delta_{21})^{\top}}{\|e_1+\delta_{21}\|}}{\|e_1+\delta_{21}\|^2}$$

which implies that $(\frac{\partial b_{21}}{\partial e_1})|_{e_f=0} = \frac{\|\delta_{21}\|^2 I_2 - \delta_{21}\delta_{21}^{\top}}{\|\delta_{21}\|^3}$ and $(\bar{e}_2\frac{\partial b_{21}}{\partial e_1})|_{e_f=0} = 0$. Then, (18) can be written as

$$\dot{e}_1 = -k_1e_1 + k_2b_{21}^*\bar{e}_2 \tag{19}$$

where $b_{21}^* = b_{21}|_{e_f=0}$. Using the same steps for $\bar{e}_2$ and $\bar{e}_3$ as (18) and (19), one has the overall linearized dynamics of (17)

$$\dot{e}_f = \left(A_1(e_f)|_{e_f=0}\right)e_f = A_1^*e_f. \tag{20}$$

Since the last column of matrix A_1^* has three zero elements, A_1^* must have one negative eigenvalue $-k_3f_{31}^* < 0$. Then, we check the remaining three eigenvalues of A_1^* which obviously are the eigenvalues of $A_2^* = \begin{bmatrix}-k_1I_2 & k_2b_{21}^* \\ k_1g_{321}^* & -k_2f_{23}^*\end{bmatrix}$. The characteristic polynomial of A_2^* is

$$\begin{aligned}|\lambda I_3 - A_2^*| &= \begin{vmatrix}\lambda + k_1 & 0 & -k_2b_{21}^*(1)\\ 0 & \lambda + k_1 & -k_2b_{21}^*(2)\\ -k_1g_{321}^*(1) & -k_1g_{321}^*(2) & \lambda + k_2f_{23}^*\end{vmatrix}\\ &= (\lambda+k_1)^2(\lambda+k_2f_{23}^*) - (\lambda+k_1)k_1k_2b_{21}^*(1)g_{321}^*(1)\\ &\quad - (\lambda+k_1)k_1k_2b_{21}^*(2)g_{321}^*(2)\\ &= (\lambda+k_1)[(\lambda+k_1)(\lambda+k_2f_{23}^*)\\ &\quad - k_1k_2(b_{21}^*(1)g_{321}^*(1) + b_{21}^*(2)g_{321}^*(2))].\end{aligned}\tag{21}$$

Note that $b_{21}^*(1)g_{321}^*(1) + b_{21}^*(2)g_{321}^*(2) = g_{321}^*b_{21}^* = \frac{b_{23}^{*T}P_{b_{21}^*}b_{21}^*}{l_{21}^*\sin\alpha_2^*} = 0$. Hence, the three eigenvalues of A_2^* are $-k_1, -k_1, -k_2f_{23}^*$, respectively, which are all negative. Therefore, one has that all the eigenvalues of A_1^* are negative, which implies that the dynamics (17) is locally and exponentially stable. Note that

$$e_2 = (l_{32}/l_{21})R(\pi - \bar{e}_2 - \alpha_2^*)(e_1 + \delta_{21}) - \delta_{32} \tag{22}$$

where $R(\theta) = \begin{bmatrix}\cos\theta & -\sin\theta\\ \sin\theta & \cos\theta\end{bmatrix}$ is the rotation matrix in 2-D. When $e_1(t) \to 0, \bar{e}_2(t) \to 0, \bar{e}_3(t) \to 0$ as $t \to \infty$, one has that $e_2(t) \to 0$ because $\frac{l_{32}(t)}{l_{21}(t)} \to \frac{\|\delta_{32}\|}{\|\delta_{21}\|}$ and $(\frac{l_{32}}{l_{21}}R(\pi - \alpha_2^*)\delta_{21} - \delta_{32}) \to \left[\frac{\|\delta_{32}\|}{\|\delta_{21}\|}R(\pi - \alpha_2^*)\delta_{21} - \delta_{32}\right] = 0$ or because of triangle's AAS theorem. Similarly, one also has $e_3(t) \to 0$.

The dynamics (17) are not globally stable because when the three agents' initial positions are collinear, $p_1(t), p_2(t), p_3(t)$ will always be collinear. In this case, (17) will not converge to the desired equilibrium $e_f = 0$. In the next subsection, we investigate the global stabilization of the first three agents' triangular formation.

B. Global Stabilization Using Two Relative Position Measurements

Different from (9)–(11) where agent 1 measures relative position and agents 2 and 3 measure bearings, we now let two agents be able to measure the relative positions such that (2)–(4) is globally achievable. Toward this end, we design the formation control laws as

$$u_1 = 0, \tag{23}$$

$$u_2 = -k_2(p_2 - p_1 - \delta_{12}) = -k_2e_2, \tag{24}$$

$$u_3 = -k_3(p_3 - p_1 - \delta_{13}) = -k_3e_3. \tag{25}$$

Theorem 2: For a three-agent formation (1) governed by the control laws (23)–(25), the formation objective (2)–(4) can be achieved and the formation errors $e_i(t), i = 1, 2, 3$ exponentially and globally converge to zero.

Proof: The error dynamics $\dot{e}_2, \dot{e}_3$ can be written as

$$\begin{bmatrix}\dot{e}_2\\ \dot{e}_3\end{bmatrix} = \begin{bmatrix}-k_2 I_2 & 0\\ 0 & -k_3 I_2\end{bmatrix}\begin{bmatrix}e_2\\ e_3\end{bmatrix} = A_3 \begin{bmatrix}e_2\\ e_3\end{bmatrix}.$$

Obviously, $A_3 \in \mathbb{R}^{4\times 4}$ is negative definite, which implies the global and exponential convergence of e_2, e_3. It follows that $e_1 = -e_2 - e_3$ also globally converges to zero.

Remark 2: In (11), agent 3 only measures bearings which guarantees a locally stable formation. Compared to (11), agent 3 measures relative position in (25) which guarantees a globally stable formation. Therefore, if more measurements are available, the convergence property of the formation becomes better.

IV. Formation Control for the Remaining Agents

In this section, to achieve (5) and (6), we first design a locally stable formation algorithm using only bearing measurements. To improve the convergence performance, we then design a globally stable formation algorithm by using extra communication channels.

A. Local Stabilization Using Only Bearing Measurements

We add agents 4–N into the existing formation step by step through the Type-I vertex addition operation (case 2) introduced in Section II-B. Note that in [17], the control algorithm designed for agents $i = 4, \ldots, N$ is

$$\begin{aligned} u_i =& -(\alpha_{j_1 i j_2} - \alpha^*_{j_1 i j_2})(b_{ij_1} + b_{ij_2})\\ &-(\alpha_{j_2 i j_3} - \alpha^*_{j_2 i j_3})(b_{ij_2} + b_{ij_3}) \end{aligned} \tag{26}$$

where $\alpha^*_{j_1 i j_2} \in (0,\pi)$ and $\alpha^*_{j_2 i j_3} \in (0,\pi)$, $j_1 < i, j_2 < i, j_3 < i$, $j_1 \neq j_2 \neq j_3$ are the two desired angles to be maintained by agent i. To guarantee the local stability for agents 4–N, the following three conditions

$$\begin{aligned} &\alpha^*_{j_3 i j_1} = \alpha^*_{j_2 i j_1} + \alpha^*_{j_3 i j_2}, \sin\alpha^*_{j_1 j_2 i} > \sin\alpha^*_{i j_1 j_2},\\ &\sin\alpha^*_{i j_2 j_3} > \sin\alpha^*_{j_2 j_3 i} \end{aligned} \tag{27}$$

are required in [17]. In this article, we aim at removing these three conditions by properly assigning control gains for the angle errors e_{i1}, e_{i2} in (26). To be specific, we modify (26) into

$$\begin{aligned} u_i =& -(\alpha_{j_1 i j_2} - \alpha^*_{j_1 i j_2})(k_{i1} b_{ij_1} + k_{i2} b_{ij_3})\\ &-(\alpha_{j_2 i j_3} - \alpha^*_{j_2 i j_3})(k_{i3} b_{ij_1} + k_{i4} b_{ij_3}), i = 4, \ldots, N \end{aligned} \tag{28}$$

where $j_1 \neq j_2 \neq j_3 < i$, and the scalars $k_{i1}, k_{i2}, k_{i3}, k_{i4}$ are constant gains. Since $\alpha_{j_1 i j_2} = \arccos(b_{ij_1}^\top b_{ij_2})$, (28) only needs the bearing measurements $b_{ij_1}, b_{ij_2}, b_{ij_3}$.

To show the N-agent formation's stability under the control of (28), we first analyze the case of agent 4, and the cases for the other agents will be similarly obtained. Thus, when $i = 4$ and $\alpha^*_{241} + \alpha^*_{342} = \alpha^*_{143}$, (28) can be specified as

$$\begin{aligned} u_4 =& -(\alpha_{241} - \alpha^*_{241})(k_{41} b_{41} + k_{42} b_{43})\\ &-(\alpha_{342} - \alpha^*_{342})(k_{43} b_{41} + k_{44} b_{43}). \end{aligned} \tag{29}$$

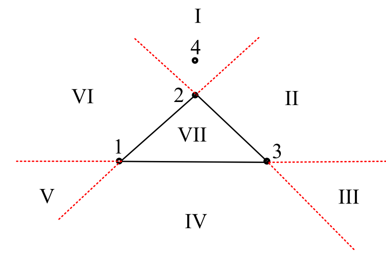

Fig. 3. Different subregions for p^*_4.

Note that the relationship of the three desired angles $\alpha^*_{241}, \alpha^*_{342}, \alpha^*_{143}$ depends on the region that p^*_4 lies at. Hence, we first divide the whole 2-D plane along the lines 12, 23, and 31 into seven open subregions which are shown in Fig. 3. When p^*_4 lies in I, one has $\alpha^*_{143} = \alpha^*_{142} + \alpha^*_{243}$; while in II, one has $\alpha^*_{243} = \alpha^*_{142} + \alpha^*_{143}$.

Note that the case of point p^*_4 lying in I (respectively II) has common properties as the case of p^*_4 lying in IV (respectively V). Therefore, we first analyze the angle error dynamics under the controller (29) and discuss the cases that point p^*_4 lies in I or IV, respectively.

1) Angle Error Dynamics:

To obtain (5) and (6), we first derive the dynamics of e_{41}, e_{42}. Using (13) and (14), one has

$$\begin{aligned} \dot{e}_{41} = \dot{\alpha}_{241} =& -\frac{\dot{b}_{41}^{\mathrm{T}} b_{42} + b_{41}^{\mathrm{T}} \dot{b}_{42}}{\sin\alpha_{241}}\\ =& \frac{\left(\frac{b_{42}^\top P_{b_{41}}}{l_{41}} + \frac{b_{41}^\top P_{b_{42}}}{l_{42}}\right) u_4 + k_1 \frac{b_{42}^\top P_{b_{41}} e_1}{l_{41}} + k_2 \frac{b_{41}^\top P_{b_{42}} b_{23}}{l_{42}} \bar{e}_2}{\sin\alpha_{241}} \end{aligned} \tag{30}$$

where we used the case that agents 1–3 are governed by (9)–(11). Then, we calculate the part in (30)

$$\frac{\left(\frac{b_{42}^\top P_{b_{41}}}{l_{41}} + \frac{b_{41}^\top P_{b_{42}}}{l_{42}}\right) u_4}{\sin\alpha_{241}} = a_{11} e_{41} + a_{12} e_{42} \tag{31}$$

where

$$\begin{aligned} a_{11} &= -\left[\frac{k_{42}\sin\alpha_{341}}{l_{41}} + \frac{k_{41}\sin\alpha_{241} - k_{42}\sin\alpha_{342}}{l_{42}}\right],\\ a_{12} &= -\left[\frac{k_{44}\sin\alpha_{341}}{l_{41}} + \frac{k_{43}\sin\alpha_{241} - k_{44}\sin\alpha_{342}}{l_{42}}\right] \end{aligned}$$

and we used $\alpha_{143} = \alpha_{142} + \alpha_{243}$ since p_4 is in I or IV. Similarly, for $e_{42} = \alpha_{342} - \alpha^*_{342}$, one has

$$\begin{aligned} \dot{e}_{42} = \dot{\alpha}_{342} =& -\frac{(\dot{b}_{42})^{\mathrm{T}} b_{43} + (b_{42})^{\mathrm{T}} \dot{b}_{43}}{\sin\alpha_{342}}\\ =& \frac{\left(\frac{b_{43}^\top P_{b_{42}}}{l_{42}} + \frac{b_{42}^\top P_{b_{43}}}{l_{43}}\right) u_4 + \frac{k_3 b_{42}^\top P_{b_{43}} b_{31}}{l_{43}}\bar{e}_3 + k_2 \frac{b_{43}^\top P_{b_{42}} b_{23}}{l_{42}}\bar{e}_2}{\sin\alpha_{342}}. \end{aligned} \tag{32}$$

Then, the first part in (32) can be calculated as

$$\frac{\left(\frac{b_{43}^\top P_{b_{42}}}{l_{42}} + \frac{b_{42}^\top P_{b_{43}}}{l_{43}}\right) u_4}{\sin\alpha_{342}} = a_{21} e_{41} + a_{22} e_{42} \tag{33}$$

where

$$a_{21} = -\left[\frac{-k_{41}\sin\alpha_{241} + k_{42}\sin\alpha_{342}}{l_{42}} + \frac{k_{41}\sin\alpha_{341}}{l_{43}}\right],$$

$$a_{22} = -\left[\frac{-k_{43}\sin\alpha_{241} + k_{44}\sin\alpha_{342}}{l_{42}} + \frac{k_{43}\sin\alpha_{341}}{l_{43}}\right].$$

Summarizing (30)–(33), one has the overall angle error dynamics

$$\begin{aligned}\dot{e}_4 &= \begin{bmatrix}\dot{e}_{41}\\ \dot{e}_{42}\end{bmatrix} = \begin{bmatrix}a_{11} & a_{12}\\ a_{21} & a_{22}\end{bmatrix}\begin{bmatrix}e_{41}\\ e_{42}\end{bmatrix} + \begin{bmatrix}c_{11} & c_{12} & c_{13}\\ c_{21} & c_{22} & c_{23}\end{bmatrix}\begin{bmatrix}e_1\\ \bar{e}_2\\ \bar{e}_3\end{bmatrix}\\ &= A_4(e_f, e_4)e_4 + C_1(e_f, e_4)e_f \qquad (34)\end{aligned}$$

where $c_{11} = k_1\frac{b_{42}^\top P_{b_{41}}}{l_{41}\sin\alpha_{241}}, c_{12} = k_2\frac{b_{41}^\top P_{b_{42}} b_{23}}{l_{42}\sin\alpha_{241}}, c_{13} = 0, c_{21} = 0, c_{22} = k_2\frac{b_{43}^\top P_{b_{42}} b_{23}}{l_{42}\sin\alpha_{342}}, c_{23} = \frac{k_3 b_{42}^\top P_{b_{43}} b_{31}}{l_{43}\sin\alpha_{342}}$. The global stability of (34) is challenging; thus, we analyze the local stability of (34). Following (18)–(20), the linearized dynamics of (34) are

$$\begin{aligned}\dot{e}_4 &= \left(A_4(e_f, e_4)|_{e_f=0, e_4=0}\right)e_4 + \left(C_1(e_f, e_4)|_{e_f=0, e_4=0}\right)e_f\\ &= A_4^* e_4 + C_1^* e_f. \qquad (35)\end{aligned}$$

Since $\lim_{t\to\infty} e_f(t) = 0$, the stability of (35) depends on the eigenvalues of $A_4^* \in \mathbb{R}^{2\times 2}$ which are determined by $\det(A_4^*)$ and $\mathrm{tr}(A_4^*)$. In other words, (35) is stable if and only if A_4^* is Hurwitz, which holds if $\det(A_4^*) > 0, \mathrm{tr}(A_4^*) < 0$. Therefore, we calculate

$$\begin{aligned}\mathrm{tr}(A_4^*) &= (a_{11} + a_{22})|_{e_f=0, e_4=0}\\ &= -\frac{k_{42}\sin\alpha_{341}^*}{l_{41}^*} - \frac{k_{43}\sin\alpha_{341}^*}{l_{43}^*}\\ &\quad - \frac{(k_{41} - k_{43})\sin\alpha_{241}^* + (k_{44} - k_{42})\sin\alpha_{342}^*}{l_{42}^*} \qquad (36)\end{aligned}$$

$$\begin{aligned}\det(A_4^*) &= (a_{11}a_{22} - a_{21}a_{12})|_{e_f=0, e_4=0}\\ &= \frac{[k_{41}k_{44} - k_{43}k_{42}]\sin\alpha_{241}^*\sin\alpha_{341}^*}{l_{41}^* l_{42}^*}\\ &\quad + \frac{[k_{41}k_{44} - k_{43}k_{42}]\sin\alpha_{341}^*\sin\alpha_{342}^*}{l_{42}^* l_{43}^*}\\ &\quad - \frac{[k_{41}k_{44} - k_{43}k_{42}]\sin\alpha_{341}^{*2}}{l_{41}^* l_{43}^*}\\ &= \frac{[k_{41}k_{44} - k_{43}k_{42}]\sin\alpha_{341}^*}{l_{41}^* l_{42}^* l_{43}^*}\phi_4 \qquad (37)\end{aligned}$$

where $\phi_4 = l_{41}^*\sin\alpha_{342}^* + l_{43}^*\sin\alpha_{241}^* - l_{42}^*\sin\alpha_{341}^*$. To obtain $\det(A_4^*) > 0$, (37) implies that ϕ_4 plays an important role. In the following, we analyze the sign of ϕ_4 for the cases of p_4^* lying in region I or region IV, respectively.

2) p_4^* Lies in the Region I:

We first present the result about ϕ_4 when p_4^* lies in region I.

Lemma 1: If p_4^* is in region I, then $\phi_4 > 0$.

The proof of this lemma can be found in Appendix A. Then, we discuss the other case that p_4^* lies in region IV.

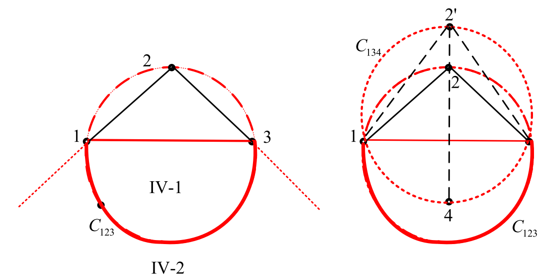

(a) (b)

Fig. 4. Splitting region IV into IV-1, IV-2, and $\mathcal{C}_{123}$.

3) p_4^* Lies in Region IV:

It is more complicated when p_4^* lies in region IV since the sign of ϕ_4 depends on the place p_4^* lies at. Denote by $\mathcal{C}_{ijk}$ the circle spanned by p_i^*, p_j^*, p_k^* and split region IV into three parts, IV-1, $\mathcal{C}_{123}$, and IV-2, which are shown in Fig. 4(a).

Lemma 2: If $p_4^* \in$ IV-1, then $\phi_4 > 0$; if $p_4^* \in \mathcal{C}_{123} \cap$ IV, then $\phi_4 = 0$; if $p_4^* \in$ IV-2, then $\phi_4 < 0$.

Proof: 1) The case $p_4^* \in \mathcal{C}_{123} \cap$ IV: In this case, p_4^* must be in arc 13 which does not include p_2^*. Since p_1^*, p_2^*, p_3^*, and p_4^* are cocircle, one has $\alpha_{213}^* = \alpha_{243}^*$, $\alpha_{142}^* = \alpha_{132}^*$, $\alpha_{143}^* = \pi - \alpha_{123}^*$, and $l_{42}^* l_{13}^* = l_{12}^* l_{43}^* + l_{14}^* l_{23}^*$ according to the Ptolemy's theorem [18]. It follows that $l_{42}^* = l_{43}^*\frac{l_{12}^*}{l_{13}^*} + l_{14}^*\frac{l_{23}^*}{l_{13}^*}$. Using the law of sines, one has $\frac{\sin\alpha_{231}^*}{l_{12}^*} = \frac{\sin\alpha_{213}^*}{l_{23}^*} = \frac{\sin\alpha_{123}^*}{l_{13}^*}$. Hence, one has

$$l_{42}^* = l_{41}^*\frac{\sin\alpha_{213}^*}{\sin\alpha_{123}^*} + l_{43}^*\frac{\sin\alpha_{132}^*}{\sin\alpha_{123}^*}$$

which implies $\phi_4 = 0$.

2) The case $p_4^* \in$ IV-1: To prove $\phi_4 > 0$, we first construct the circle $\mathcal{C}_{143}$. As shown in Fig. 4(b), denote by R' the radius of the circle $\mathcal{C}_{143}$ and denote by 2' the intersection of $\mathcal{C}_{143}$ and the ray $\overrightarrow{42}$. Then, one has

$$\begin{aligned}2R'\phi_4 &= l_{41}^*(2R'\sin\alpha_{342}^*) + l_{43}^*(2R'\sin\alpha_{241}^*)\\ &\quad - l_{42}^*(2R'\sin\alpha_{341}^*)\\ &= l_{41}^* l_{32'}^* + l_{43}^* l_{12'}^* - l_{42}^* l_{31}^* = (l_{42'}^* - l_{42}^*)l_{31}^*. \qquad (38)\end{aligned}$$

Since p_4^* lies in IV-1, one has that $l_{42'}^* > l_{42}^*$ which implies that $2R'\phi_4 > 0$ and $\phi_4 > 0$.

3) The case $p_4^* \in$ IV-2: For this case, one can also construct a circle $\mathcal{C}_{134}$. Denote by R'' the radius of the circle $\mathcal{C}_{134}$ and denote by 2" the intersection of $\mathcal{C}_{134}$ and the segment $\overline{24}$. Then, one has

$$\begin{aligned}2R''\phi_4 &= l_{41}^*(2R''\sin\alpha_{342}^*) + l_{43}^*(2R''\sin\alpha_{241}^*)\\ &\quad - l_{42}^*(2R''\sin\alpha_{341}^*)\\ &= l_{41}^* l_{32''}^* + l_{43}^* l_{12''}^* - l_{42}^* l_{31}^* = (l_{42''}^* - l_{42}^*)l_{31}^* \qquad (39)\end{aligned}$$

which implies that $\phi_4 < 0$ because $l_{42''}^* < l_{42}^*$.

After obtaining the relationship between the sign of ϕ_4 and the place p_4^* lies at in Lemmas 1 and 2, we are ready to tune the gains $k_{41}, k_{42}, k_{43}, k_{44}$ in (29) such that A_4^* is Hurwitz.

Theorem 3: When Assumption 1 holds and p_4^* lies in region I or IV, if one selects $k_{42} > 0, k_{43} > 0$ and

$$\begin{cases} k_{41} > k_{43}, k_{44} > k_{42}, \text{if } \phi_4 > 0 \\ (k_{41}k_{44} - k_{42}k_{43}) < 0, \text{if } \phi_4 < 0 \end{cases} \tag{40}$$

then A_4^* is Hurwitz and the angle error dynamics (34) is locally and exponentially stable.

Proof.

Note that when Assumption 1 holds, $\phi_4 \neq 0$. Therefore, we only need to prove that the selected gains in (40) can guarantee $\text{tr}(A_4^*) < 0$ and $\det(A_4^*) > 0$.

1) The case $\phi_4 > 0$: By selecting $k_{41} > k_{43} > 0, k_{44} > k_{42} > 0$ in (40), one has $k_{41}k_{44} - k_{43}k_{42} > 0$. According to (36) and (37), $\text{tr}(A_4^*) < 0$, $\det(A_4^*) > 0$ which implies that A_4^* is Hurwitz.

2) The case $\phi_4 < 0$: Using the gain selection in (40), one has $k_{41}k_{44} - k_{43}k_{42} < 0$ which implies $\det(A_4^*) > 0$. We then prove $\text{tr}(A_4^*) < 0$. Multiplying $\text{tr}(A_4^*)$ by $l_{41}^* l_{42}^* l_{43}^*$ in (36) yields

$$\begin{aligned} l_{41}^* l_{42}^* l_{43}^* \text{tr}(A_4^*) &= -(k_{42} l_{43}^* + k_{43} l_{41}^*) l_{42}^* \sin \alpha_{341}^* \\ &\quad - l_{41}^* l_{43}^* [(k_{41} - k_{43}) \sin \alpha_{241}^* + (k_{44} - k_{42}) \sin \alpha_{342}^*]. \end{aligned} \tag{41}$$

Since $k_{42} > 0, k_{43} > 0$, one has $k_{42} l_{43}^* + k_{43} l_{21}^* > 0$. Using the fact $\phi_4 < 0$, one has

$$\begin{aligned} &(k_{42} l_{43}^* + k_{43} l_{41}^*) l_{42}^* \sin \alpha_{341}^* > (k_{42} l_{43}^* + k_{43} l_{41}^*) \\ &\times (l_{41}^* \sin \alpha_{342}^* + l_{43}^* \sin \alpha_{241}^*) \\ &= l_{41}^* l_{43}^* \bigg(k_{42} \sin \alpha_{342}^* + k_{43} \sin \alpha_{241}^* \\ &\qquad + \frac{k_{42} l_{43}^*}{l_{41}^*} \sin \alpha_{241}^* + \frac{k_{43} l_{41}^*}{l_{43}^*} \sin \alpha_{342}^* \bigg). \end{aligned}$$

Thus, (41) can be further written as

$$\begin{aligned} l_{41}^* l_{42}^* l_{43}^* \text{tr}(A_4^*) &< -l_{41}^* l_{43}^* \bigg(k_{42} \sin \alpha_{342}^* + k_{43} \sin \alpha_{241}^* \\ &\qquad + \frac{k_{42} l_{43}}{l_{41}^*} \sin \alpha_{241}^* + \frac{k_{43} l_{41}^*}{l_{43}^*} \sin \alpha_{342}^* \bigg) \\ &\quad - l_{41}^* l_{43}^* [(k_{41} - k_{43}) \sin \alpha_{241}^* + (k_{44} - k_{42}) \sin \alpha_{342}^*] \\ &= -l_{41}^* l_{43}^* \bigg[\frac{k_{42} l_{43}^*}{l_{41}^*} \sin \alpha_{241}^* + \frac{k_{43} l_{41}^*}{l_{43}^*} \sin \alpha_{342}^* \\ &\qquad + k_{41} \sin \alpha_{241}^* + k_{44} \sin \alpha_{342}^* \bigg] < 0 \end{aligned} \tag{42}$$

which implies $\text{tr}(A_4^*) < 0$. Combining the above two cases, one has that A_4^* is Hurwitz under (40).

Note that the cases of p_4^* lying in region I or IV are discussed in Theorem 3. When p_4^* lies in region II, III, V, VI, or VII, one can always adjust the order of the agents such that the designed control laws still work. More specifically, if $p_4^* \in \text{V} \cup \text{II}$ or $\alpha_{241}^* + \alpha_{143}^* = \alpha_{243}^*$, (28) can be specified as $j_1 = 2, j_2 = 1, j_3 = 3$. Moreover, if $p_4^* \in \text{VII}$, then the first triangular shape becomes $\triangle 142$ and the next two desired angles to be achieved become $\alpha_{134}^*, \alpha_{432}^*$. To further illustrate the gain design technique employed to guarantee the stability of the four-agent formation, we summarize the gain design procedure provided in this subsection as Algorithm 1.

Algorithm 1: Assign Control Gains for Agent 4's Controller (28).

Given three desired angles $\alpha_{142}^* \in (0, \pi)$,$\alpha_{243}^* \in (0, \pi)$, $\alpha_{143}^* \in (0, \pi)$ and desired distances $l_{41}^*, l_{42}^*, l_{43}^* > 0$;
if $\alpha_{143}^* = \alpha_{142}^* + \alpha_{243}^*$ **then**
  $j_1 = 1, j_2 = 2, j_3 = 3$;
else
  if $\alpha_{243}^* = \alpha_{241}^* + \alpha_{143}^*$ **then**
    $j_1 = 2, j_2 = 1, j_3 = 3$;
  else
    if $\alpha_{142}^* = \alpha_{243}^* + \alpha_{143}^*$ **then**
      $j_1 = 1, j_2 = 3, j_3 = 2$;
    end
  end
end
$\phi_4 = l_{4j_1}^* \sin \alpha_{j_3 4 j_2}^* + l_{4j_3}^* \sin \alpha_{j_2 4 j_1}^* - l_{4j_2}^* \sin \alpha_{j_3 4 j_1}^*$;
if $\phi_4 > 0$ **then**
  Assign $k_{41} > k_{43} > 0, k_{44} > k_{42} > 0$
else
  if $\phi_4 < 0$ **then**
    Assign $k_{43} > 0, k_{42} > 0, k_{41}k_{44} < k_{42}k_{43}$
  else
    Output 'infeasible/non-generic formation'
  end
end

Now, we extend the results to the N-agent formation case. For an arbitrary agent $i, 4 \leq i \leq N$, the control gains in (28) can be selected as

$$\begin{cases} k_{i1} > k_{i3} > 0, k_{i4} > k_{i2} > 0, \text{if } \phi_i > 0 \\ (k_{i1}k_{i4} - k_{i2}k_{i3}) < 0, k_{i2} > 0, k_{i3} > 0, \text{if } \phi_i < 0 \end{cases} \tag{43}$$

where $\phi_i = l_{ij_1}^* \sin \alpha_{j_3 i j_2}^* + l_{ij_3}^* \sin \alpha_{j_2 i j_1}^* - l_{ij_2}^* \sin \alpha_{j_3 i j_1}^*$.

Proposition 1: Consider an N-agent formation with the first three agents governed by (9)–(11) and the remaining agents governed by (28). If Assumption 1 holds and the control gains are selected as (43), then the desired N-agent formation is achieved with prescribed orientation $\frac{\delta_{21}}{\|\delta_{21}\|}$ and scale $\|\delta_{21}\|$ and the errors in (2)–(6) locally converge to zero.

The proof of Proposition 1 follows the induction since the N-agent formation is constructed in a cascading way. Based on [17], [19], the local stability of the N-agent formation can be obtained. Also, the gain design procedure for agent i, with $5 < i \leq N$, can be similarly obtained following Algorithm 1. Instead of local stability, the next subsection globally stabilizes the formation using additional communication.

Remark 3: The structure of the proposed controller (28) is different from the controller (26) proposed in [17]. The inequalities (27) cannot be avoided if one applies the gain design technique directly into the controller (26). Although the design of the control gains given in Algorithm 1 and the formation design in Fig. 1 is centralized, the execution of the formation controller

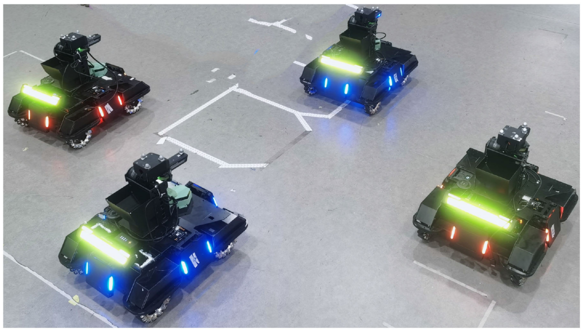

Fig. 5. Four wheeled robots.

is distributed since all the agents move simultaneously using the measurements with respect to only their neighbors.

B. Global Stabilization Using Bearing Measurements and Interagent Communication

Since the first three agents' formation is globally and exponentially stable under (23)-(25), we now aim at designing globally stable control law for agents 4–N based on Type-I (case 1) vertex addition operation.

Specifically, we design the control law as

$$u_i = (\alpha_{ij_1j_2} - \alpha^*_{ij_1j_2})b_{ij_2} + (\alpha_{ij_2j_1} - \alpha^*_{ij_2j_1})b_{ij_1}. \quad (44)$$

For agent 4, the controller (44) can be specified as

$$u_4 = (\alpha_{412} - \alpha^*_{412})b_{42} + (\alpha_{421} - \alpha^*_{421})b_{41} = \bar{e}_{41}b_{42} + \bar{e}_{42}b_{41} \quad (45)$$

where $\alpha_{412} = \arccos(b_{14}^\top b_{12})$ can be obtained by agent 1 through bearing measurements and can be sent to agent 4 via wireless communication. We discuss the case for agent 4 and the remaining agents' cases can be similarly obtained.

Theorem 4: If agents 1 and 2 are fixed, agent 4 is governed by (45), and $p_4(0), p_1(0), p_2(0)$ are noncollinear, then the angle errors $\bar{e}_{41}$, $\bar{e}_{42}$ globally converge to zero.

The proof of this theorem can be found in Appendix B.

Remark 4: In Theorem 4, agents 1 and 2 are assumed to be static, without which the global convergence cannot be guaranteed. Several proposed formation controllers use bearing measurements which require the interagent collision-free property. Theoretically, the property can be obtained by following the analysis on local convergent formation's interagent distance change in [17]. Physically, the collision avoidance can be fulfilled due to agents' practical dimensions or by equipping low-level proximity sensor.

V. EXPERIMENTS

In this section, we validate the results of Theorems 1-4 using four wheeled robots to achieve a desired rectangular formation.

The size of each robot in Fig. 5 is 60 cm in length, 46 cm in width, and 46 cm in height. Each robot has four wheels and is controlled by an on-board computer. Since wheeled robots are unicycles, we apply feedback linearization [20], [21] toward a reference point that is inside of the robot to obtain the single-integrator dynamics (1). The measurements of relative positions or bearings among robots are captured by the NOKOV Mocap system sampling at the rate of 120 Hz. Each robot will calculate the control input along its X-axis and Y-axis according to the designed controllers and then apply it to the robots.

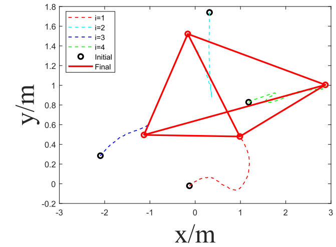

Fig. 6. Formation trajectories.

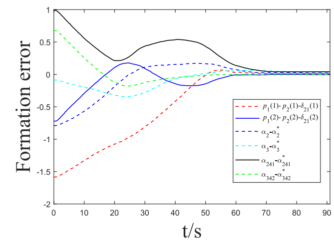

Fig. 7. Evolution of formation errors.

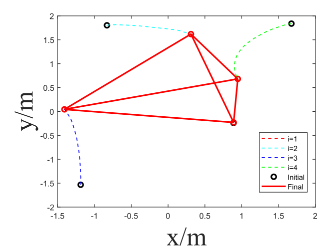

Fig. 8. Formation trajectories of the robots.

A. Formation Experiment With Local Stabilization

This experiment validates the results of Theorems 1 and 3 where the formation is proved to be locally stable. The desired formation in this experiment is described by $\delta_{21} = [1.14; -1.04], \alpha^*_2 = \pi/2, \alpha^*_3 = \pi/4, \alpha^*_{241} = 0.4, \alpha^*_{342} = 0.3, \alpha^*_{241} = \alpha^*_{342} + \alpha^*_{341}$, and the control gains are selected according to Algorithm 1 as $k_{4i} = i, i = 1, \ldots, 4$. Under the controllers (9)–(11) and (28), the formation trajectories and angle errors are shown in Figs. 6 and 7, respectively, from which one has that the formation errors almost converge to zero, and the desired formation is achieved within 75 s.

B. Formation Experiment With Global Stabilization

We validate the results of Theorems 2 and 4 in this experiment. The desired formation is described by $\delta_{12} = [-0.54; 1.84], \delta_{13} = [-2.34; 0.32], \alpha^*_{412} = 0.4, \alpha^*_{421} = 0.3$. Under the controllers (23)–(25) and (45), the formation trajectories and angle errors are shown in Figs. 8 and 9, respectively. According to Figs. 8 and 9, the desired formation

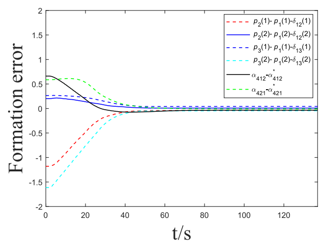

Fig. 9. Evolution of formation errors.

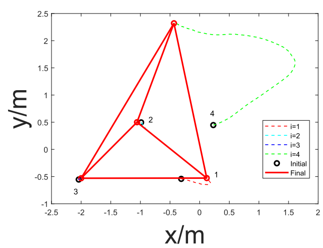

Fig. 10. Formation trajectories of the robots.

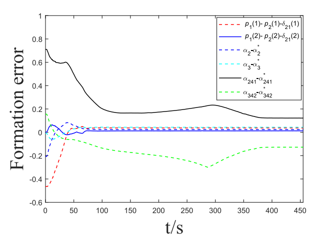

Fig. 11. Evolution of formation errors.

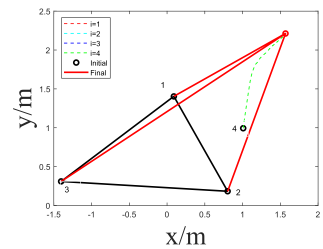

Fig. 12. Formation trajectories of the robots.

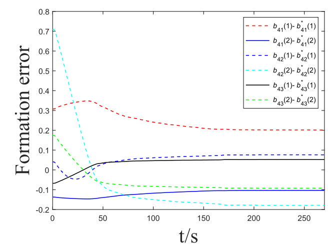

Fig. 13. Evolution of formation errors.

TABLE I
COMPARISON OF DIFFERENT FORMATION STRATEGIES

Strategies \ Properties	O	R	D
This paper	fixed	yes	all generic formations
[17]	unfixed	yes	part of generic formations
[22]	fixed	no	all generic formations

In the table, O refers to the orientation and scale of the formation, R the robustness against misalignment of agents' coordinate frames, and D the desired formations that can be stabilized.

is achieved and the formation errors almost converge to zero within 45 s, which is faster than the experiment with local stabilization. The small convergent error in Figs. 7 and 9 is due to the existence of minimum commanding threshold applicable to the robots.

C. Comparison With Other Formation Control Strategies

To further verify the advantages of the control gain design technique and the robustness against misalignment of agents' coordinate frames in our proposed controller, we conduct comparative experiments by comparing our controller with the other two most related formation control strategies proposed in [15, (2)] and [17, (45)], respectively.

For the first case in [17, (45)], we initialize all the agents the same positions as those given in the experiment of Section V-A. Then, the formation results in Figs. 10 and 11 show that the desired formation is not achieved and the formation errors associated with agent 4 do not converge to zero due to the violation of the required assumptions (27). However, under our proposed control gain design technique, the desired formation is achieved in Figs. 6 and 7.

For the second case, we initialize the first three agents as stationary as required in [15, (2)]. Note that in [15], all agents' coordinate frames should have the same orientation. Now, we add 10° misalignment in agent 4's coordinate frame. The formation results in Figs. 12 and 13 show that the desired formation described by desired bearings is not achieved and the formation errors do not converge to zero. However, adding the same misalignment into the experiment of Section V-A, the formation trajectories and the evolution of angle errors keep the same.

The conclusion obtained from these comparison cases are summarized in Table I.

VI. CONCLUSION

In this article, formation control algorithms were proposed to stabilize angle rigid formations with prescribed orientation and scale, where both advantages of requiring less sensor measurements and sustaining robustness against noise were obtained. First, we used the relative position and bearing measurements for the first three agents to achieve a desired triangular formation with prescribed orientation and scale. Then, by using a control gain design technique, a general control algorithm was proposed for the remaining agents. The role of generic property was used for the stability analysis. Experiment results validated the effectiveness and advantages of the proposed formation algorithms. Future work will concentrate on the double-integrator formations.

Appendix A
Proof of Lemma 1

When p_4^* lies in the region I, p_2^* will always be inside of the $\triangle 413$. Then, p_2^* can be written as a unique convex combination of the three points p_1^*, p_4^*, p_3^*, i.e., $\exists \varepsilon_1, \varepsilon_2, \varepsilon_3 \in (0,1)$ and $\varepsilon_1 + \varepsilon_2 + \varepsilon_3 = 1$ such that $p_2^* = \varepsilon_1 p_1^* + \varepsilon_2 p_4^* + \varepsilon_3 p_3^*$. It follows that

$$p_2^* - p_4^* = p_{42}^* = \varepsilon_1(p_1^* - p_4^*) + \varepsilon_3(p_3^* - p_4^*) = \varepsilon_1 p_{41}^* + \varepsilon_3 p_{43}^*$$

where $\varepsilon_1, \varepsilon_3 \in (0,1)$ and $0 < \varepsilon_1 + \varepsilon_3 < 1$. On the one hand, one has

$$\begin{aligned} l_{42}^{*2} &= \|\varepsilon_1 p_{41}^* + \varepsilon_3 p_{43}^*\|^2 \\ &= \varepsilon_1^2 l_{41}^{*2} + \varepsilon_3^2 l_{43}^{*2} + 2\varepsilon_1\varepsilon_3 l_{41}^* l_{43}^* \cos\alpha_{143}^* \end{aligned} \tag{46}$$

where $p_{ij} = p_j - p_i$. Using the fact (46), one has

$$\cos\alpha_{142}^* = \frac{p_{42}^{*\top} p_{41}^*}{l_{42}^* l_{41}^*} = \frac{\varepsilon_1 l_{41}^* + \varepsilon_3 l_{43}^* \cos\alpha_{143}^*}{l_{42}^*}. \tag{47}$$

Since $0 < \sin\alpha_{142}^* < 1$, it follows from (47) and (46) that

$$\sin\alpha_{142}^* = \sqrt{1 - \cos^2\alpha_{142}^*} = \varepsilon_3 l_{43}^* \sin\alpha_{143}^* / l_{42}^*. \tag{48}$$

By using similar steps from (47) and (48), one also has

$$\sin\alpha_{342}^* = (\varepsilon_1 l_{41}^* \sin\alpha_{143}^*)/l_{42}^*. \tag{49}$$

On the other hand, since $0 < \varepsilon_1 + \varepsilon_3 = 1 - \varepsilon_2 < 1$ and $0 < \cos^2\alpha_{143}^* < 1$, one has $1 - \varepsilon_1 - \varepsilon_3 + \varepsilon_1\varepsilon_3(1 - \cos^2\alpha_{143}^*) > 0$ which implies that

$$(1-\varepsilon_1)(1-\varepsilon_3) - \varepsilon_1\varepsilon_3\cos^2\alpha_{143}^* > 0. \tag{50}$$

It follows from (50) that

$$2\sqrt{\varepsilon_1\varepsilon_3(1-\varepsilon_1)(1-\varepsilon_3)}\, l_{41}^* l_{43}^* > 2\varepsilon_1\varepsilon_3 l_{41}^* l_{43}^* \cos\alpha_{143}^* \tag{51}$$

where we used the fact that $\varepsilon_i \in (0,1), i = 1,2,3$. Based on (51), one has

$$\begin{aligned} &(\sqrt{\varepsilon_1(1-\varepsilon_1)}\, l_{41}^* - \sqrt{\varepsilon_3(1-\varepsilon_3)}\, l_{43}^*)^2 \\ &+ 2\sqrt{\varepsilon_1\varepsilon_3(1-\varepsilon_1)(1-\varepsilon_3)}\, l_{41}^* l_{43}^* - 2\varepsilon_1\varepsilon_3 l_{41}^* l_{43}^* \cos\alpha_{143}^* > 0 \end{aligned}$$

which implies that

$$\varepsilon_1(1-\varepsilon_1) l_{41}^{*2} + \varepsilon_3(1-\varepsilon_3) l_{43}^{*2} - 2\varepsilon_1\varepsilon_3 l_{41}^* l_{43}^* \cos\alpha_{143}^* > 0. \tag{52}$$

It follows from (52) and (46) that

$$\varepsilon_1 l_{41}^{*2} + \varepsilon_3 l_{43}^{*2} > \varepsilon_1^2 l_{41}^{*2} + \varepsilon_3 l_{43}^{*2} + 2\varepsilon_1\varepsilon_3 l_{41}^* l_{43}^* \cos\alpha_{143}^* = l_{42}^{*2}. \tag{53}$$

Substituting (48) and (49) into (53), one has $\phi_4 > 0$. □

Appendix B
Proof of Theorem 4

Substituting the controller (45) into the calculation equation of angle error dynamics (14) yields

$$\dot{\bar{e}}_{41} = -(\dot{b}_{14}^{\mathrm{T}} b_{12} + b_{14}^{\mathrm{T}} \dot{b}_{12})/\sin\alpha_{412} = -(\sin\alpha_{142}/l_{14})\bar{e}_{41}. \tag{54}$$

Similarly, one also has

$$\dot{\bar{e}}_{42} = -(\dot{b}_{24}^{\mathrm{T}} b_{21} + b_{24}^{\mathrm{T}} \dot{b}_{21})/\sin\alpha_{421} = -(\sin\alpha_{142}/l_{24})\bar{e}_{42}. \tag{55}$$

First, we prove that $p_4(t), p_1, p_2$ will not be collinear or overlapping $\forall t > 0$. Suppose, on the contrary, that $p_4(t), p_1(t), p_2(t)$ are collinear at $t \to T_1^- > 0$. Without loss of generality, we consider the collinearity as $\alpha_{142}(T_1^-) \to \pi, \alpha_{124}(T_1^-) \to 0, \alpha_{214}(T_1^-) \to 0$. Then it follows that $\bar{e}_{41}(T_1^-) < 0, \bar{e}_{42}(T_1^-) < 0$. Using (54) and (55), one has $\dot{\bar{e}}_{41}(T_1^-) > 0, \dot{\bar{e}}_{42}(T_1^-) > 0$ which implies that $\alpha_{124}(t), \alpha_{214}(t)$ will increase. However, the hypothesis of collinearity implies that $\alpha_{124}(t), \alpha_{214}(t)$ will decrease when $t \to T_1^-$. This contradiction implies that no collinearity will occur for $\forall t > 0$. Using similar steps, one can also obtain that agents 1, 2, and 4 will not collide $\forall t > 0$.

Then, we prove that $\sin\alpha_{142}(t), l_{41}(t), l_{42}(t)$ will be upper and lower bounded. Since no collinearity and collision will happen among agents 1, 2, and 4, the dynamics (54) imply that $\bar{e}_{41}$ will decrease monotonously. Therefore, one has

$$\begin{aligned} 0 &< \min\{\alpha_{412}(0), \alpha_{412}^*\} \\ &\le \alpha_{412}(t) \le \max\{\alpha_{412}(0), \alpha_{412}^*\} < \pi. \end{aligned}$$

The same case applies for $\alpha_{421}(t)$, i.e.,

$$\begin{aligned} 0 &< \min\{\alpha_{421}(0), \alpha_{421}^*\} \\ &\le \alpha_{421}(t) \le \max\{\alpha_{421}(0), \alpha_{421}^*\} < \pi. \end{aligned}$$

It follows that

$$\begin{aligned} &0 < \pi - \max\{\alpha_{412}(0), \alpha_{412}^*\} \\ &- \max\{\alpha_{421}(0), \alpha_{421}^*\} \le \alpha_{142}(t) \\ &\le \pi - \min\{\alpha_{412}(0), \alpha_{412}^*\} - \min\{\alpha_{421}(0), \alpha_{421}^*\} < \pi. \end{aligned}$$

Therefore, the angles $\alpha_{412}(t), \alpha_{421}(t)$, and $\alpha_{142}(t)$ are all bounded away from zero and π. Then, we analyze the bounds of $l_{41}(t)$ and $l_{42}(t)$. Using the law of sines, one has

$$0 < \frac{l_{12}\sin\alpha_{421}^{\text{lower}}}{\sin\alpha_{142}^{\text{upper}}} \le l_{41}(t) = \frac{l_{12}\sin\alpha_{421}(t)}{\sin\alpha_{142}(t)} \le \frac{l_{12}\sin\alpha_{421}^{\text{upper}}}{\sin\alpha_{142}^{\text{lower}}}$$

where $\sin\alpha_{421}^{\text{lower}} = \min\{\sin\alpha_{421}(0), \sin\alpha_{421}^*\}, \sin\alpha_{421}^{\text{upper}} = \max\{\sin\alpha_{421}(0), \sin\alpha_{421}^*, 1\}, \sin\alpha_{142}^{\text{upper}} = \max\{\sin\alpha_{142}(0), \sin\alpha_{142}^*, 1\}, \sin\alpha_{142}^{\text{lower}} = \min\{\sin\alpha_{142}(0), \sin\alpha_{142}^*\}$. Similarly, one has $0 < \frac{l_{12}\sin\alpha_{412}^{\text{lower}}}{\sin\alpha_{142}^{\text{upper}}} \le l_{42}(t) \le \frac{l_{12}\sin\alpha_{412}^{\text{upper}}}{\sin\alpha_{142}^{\text{lower}}} < \infty$ where $\sin\alpha_{412}^{\text{lower}} = \min\{\sin\alpha_{412}(0), \sin\alpha_{412}^*\}, \sin\alpha_{412}^{\text{upper}} = \max\{\sin\alpha_{412}(0), \sin\alpha_{412}^*, 1\}$. Write (54) and (55) into a compact form

$$\begin{bmatrix} \dot{\bar{e}}_{41} \\ \dot{\bar{e}}_{42} \end{bmatrix} = -W(t)W^\top(t) \begin{bmatrix} \bar{e}_{41} \\ \bar{e}_{42} \end{bmatrix} \tag{56}$$

where $W(t) = \begin{bmatrix} \sqrt{\frac{\sin\alpha_{142}}{l_{14}}} & 0 \\ 0 & \sqrt{\frac{\sin\alpha_{142}}{l_{24}}} \end{bmatrix}$. Then, for every $t > 0$, $\beta_1 I_2 \le \int_t^{t+T} W(\tau)W^\top(\tau)\mathrm{d}\tau \le \beta_2 I_2$ where $T > 0$

$$\beta_1 = \frac{(\sin\alpha_{142}^{\text{lower}})^2 T}{l_{12}\max\{\sin\alpha_{421}^{\text{upper}}, \sin\alpha_{412}^{\text{upper}}\}},$$

$$\beta_2 = \frac{(\sin\alpha_{142}^{\text{upper}})^2 T}{l_{12}\min\{\sin\alpha_{421}^{\text{lower}}, \sin\alpha_{412}^{\text{lower}}\}}.$$

Using [22, Theorem 2.5.1], $\bar{e}_{41}(t), \bar{e}_{42}(t)$ converge to zero globally and exponentially. $\square$

References

[1] A. Yufka and M. Ozkan, "Formation-based control scheme for cooperative transportation by multiple mobile robots," *Int. J. Adv. Robot. Syst.*, vol. 12, no. 9, p. 120, 2015.

[2] H. Ahn, D.-T. Le, D. T. Nguyen, and H. Choo, "Real-time drone formation control for group display," in *Proc. Int. Conf. Ubiquitous Inf. Manage. Commun.*, Cham, Switzerland: Springer, 2019, pp. 778–785.

[3] G. Krieger, I. Hajnsek, K. P. Papathanassiou, M. Younis, and A. Moreira, "Interferometric synthetic aperture radar (SAR) missions employing formation flying," *Proc. IEEE*, vol. 98, no. 5, pp. 816–843, May 2010.

[4] K.-K. Oh, M.-C. Park, and H.-S. Ahn, "A survey of multi-agent formation control," *Automatica*, vol. 53, pp. 424–440, 2015.

[5] H. G. de Marina, "Maneuvering and robustness issues in undirected displacement-consensus-based formation control," *IEEE Trans. Autom. Control*, vol. 66, no. 7, pp. 3370–3377, Jul. 2021.

[6] S. Zhao and D. Zelazo, "Bearing rigidity and almost global bearing-only formation stabilization," *IEEE Trans. Autom. Control*, vol. 61, no. 5, pp. 1255–1268, May 2016.

[7] G. Jing, G. Zhang, H. W. J. Lee, and L. Wang, "Angle-based shape determination theory of planar graphs with application to formation stabilization," *Automatica*, vol. 105, pp. 117–129, 2019.

[8] Z. Sun, "Distributed stabilization control of rigid formations with prescribed orientations," in *Cooperative Coordination and Formation Control for Multi-agent Systems*. Berlin, Germany: Springer, 2018, pp. 81–99.

[9] C. Wang, H. Tnunay, Z. Zuo, B. Lennox, and Z. Ding, "Fixed-time formation control of multirobot systems: Design and experiments," *IEEE Trans. Ind. Electron.*, vol. 66, no. 8, pp. 6292–6301, Aug. 2019.

[10] Z. Meng, B. D. Anderson, and S. Hirche, "Formation control with mismatched compasses," *Automatica*, vol. 69, pp. 232–241, 2016.

[11] L. Krick, M. E. Broucke, and B. A. Francis, "Stabilisation of infinitesimally rigid formations of multi-robot networks," *Int. J. Control*, vol. 82, no. 3, pp. 423–439, 2009.

[12] H.-S. Ahn, *Formation Control: Approaches for Distributed Agents*, vol. 205. Berlin, Germany: Springer, 2019, pp. 31–49.

[13] Z. Sun, H. G. de Marina, G. S. Seyboth, B. D. Anderson, and C. Yu, "Circular formation control of multiple unicycle-type agents with non-identical constant speeds," *IEEE Trans. Control Syst. Technol.*, vol. 27, no. 1, pp. 192–205, Jan. 2019.

[14] R. Olfati-Saber and R. M. Murray, "Graph rigidity and distributed formation stabilization of multi-vehicle systems," in *Proc. 41st IEEE Conf. Decis. Control*, vol. 3, 2002, pp. 2965–2971.

[15] S. Zhao, Z. Li, and Z. Ding, "Bearing-only formation tracking control of multiagent systems," *IEEE Trans. Autom. Control*, vol. 64, no. 11, pp. 4541–4554, Nov. 2019.

[16] S. Zhao and D. Zelazo, "Bearing rigidity theory and its applications for control and estimation of network systems: Life beyond distance rigidity," *IEEE Control Syst. Mag.*, vol. 39, no. 2, pp. 66–83, Apr. 2019.

[17] L. Chen, M. Cao, and C. Li, "Angle rigidity and its usage to stabilize multi-agent formations in 2-D," *IEEE Trans. Autom. Control*, vol. 66, no. 8, pp. 3667–3681, Aug. 2021.

[18] G. I. S. Amarasinghe, "A concise elementary proof for the Ptolemy's theorem," *Glob. J. Adv. Res. Classical Modern Geometries*, vol. 2, no. 1, pp. 20–25, 2013.

[19] H. K. Khalil, *Nonlinear Systems*, vol. 3. Upper Saddle River, NJ, USA: Prentice Hall, 2002, pp. 174–175.

[20] S. Zhao and Z. Sun, "Defend the practicality of single-integrator models in multi-robot coordination control," in *Proc. 13th IEEE Int. Conf. Control Automat.*, 2017, pp. 666–671.

[21] H. Tnunay, Z. Li, C. Wang, and Z. Ding, "Distributed collision-free coverage control of mobile robots with consensus-based approach," in *Proc. 13th IEEE Int. Conf. Control Automat.*, 2017, pp. 678–683.

[22] S. Sastry and M. Bodson, *Adaptive Control: Stability, Convergence and Robustness*. Chelmsford, MA, USA: Courier Corporation, 2011, pp. 71–72.

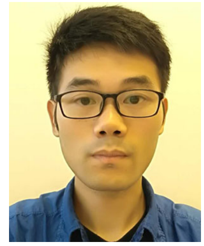

Liangming Chen (Member, IEEE) received the B.E. degree in automation from Southwest Jiaotong University, Chengdu, China, in 2015.

From 2015 to 2021, he has been enrolled jointly in the Ph.D. programs of system control in the Harbin Institute of Technology, Harbin, China, and the University of Groningen, Groningen, The Netherlands. He is currently a Research Fellow with the School of Mechanical and Aerospace Engineering, Nanyang Technological University, Singapore. His current research interests are in formation control and multiagent systems.

Qingkai Yang (Member, IEEE) received the first Ph.D. degree in control science and engineering from the Beijing Institute of Technology, Beijing, China, in 2018, and the second Ph.D. degree in system control from the University of Groningen, Groningen, The Netherlands, in 2018.

He is currently an Assistant Professor with the School of Automation, Beijing Institute of Technology. His research interest is in cooperative control of multiagent systems and autonomous agents.

Mingming Shi received the B.Eng. and M.Eng. degrees both in aerospace from the Harbin Institute of Technology, Harbin, China, in 2013 and 2015, respectively, and the Ph.D. degree in control theory from the University of Groningen, Groningen, The Netherlands, in 2019.

He is currently a Postdoctoral Researcher with the Universite Catholique de Louvain, Ottignies-Louvain-la-Neuve, Belgium. His research interests include networked systems and sensor networks.

Yanan Li received the M.Eng. degree in control science and engineering from the Harbin Institute of Technology, Harbin, China, in 2019. where she is currently working toward the Ph.D. degree also in control science and engineering.

Her research interest is in cooperative control and AUV path planning.

Mir Feroskhan received B.E. degree in aerospace engineering from Nanyang Technological University (NTU), Singapore, in 2011, and the Ph.D. degree in aerospace engineering from the Florida Institute of Technology, Melbourne, FL, USA, in 2016.

He is currently an Assistant Professor with the School of Mechanical & Aerospace Engineering, NTU. His research interests include nonlinear control systems, flight dynamics and control, and aerial robotics.